



A computationally efficient simulation model for estimating energy consumption of electric vehicles in the context of route planning applications



Konstantinos N. Genikomsakis ^{a,b,*}, Georgios Mitrentsis ^c

^a DeustoTech – Deusto Foundation, Avda Universidades, 24, 48007 Bilbao, Spain

^b Faculty of Engineering, University of Deusto, Avda Universidades, 24, 48007 Bilbao, Spain

^c Department of Electrical and Computer Engineering, Aristotle University of Thessaloniki, University Campus, Egnatia Str., 54124 Thessaloniki, Greece

ARTICLE INFO

Article history:

Available online 9 November 2016

Keywords:

Electric vehicle
Energy consumption
Driving cycle
EV performance

ABSTRACT

The fact that electric vehicles (EVs) are characterized by relatively short driving range not only signifies the importance of routing applications to compute energy efficient or optimal paths, but also underlines the necessity for realistic simulation models to estimate the energy consumption of EVs. To this end, the present paper introduces an accurate yet computationally efficient energy consumption model for EVs, based on generic high-level specifications and technical characteristics. The proposed model employs a dynamic approach to simulate the energy recuperation capability of the EV and takes into account motor overload conditions to represent the vehicle performance over highly demanding route sections. To validate the simulation model developed in this work, its output over nine typical driving cycles is compared to that of the Future Automotive Systems Technology Simulator (FASTSim), which is a simulation tool tested on the basis of real-world data from existing vehicles. The validation results show that the mean absolute error (MAE) of cumulative energy consumption is less than 45 W h on average, while the computation time to perform each driving cycle is of the order of tens of milliseconds, indicating that the developed model strikes a reasonable balance between efficacy of representation and computational efficiency. Comprehensive simulation results are presented in order to exemplify the key features of the model and analyze its output under specific highly aggressive driving cycles for road gradients ranging from -6% to 6%, in support of its usability as a practical solution for estimating the energy consumption in EV routing applications.

© 2016 Elsevier Ltd. All rights reserved.

1. Introduction

Electric vehicles (EVs) are typically viewed as a promising pathway to decarbonize the transportation sector in the long-term, given that the electrification of passenger vehicles bears the potential to reduce carbon emissions and dependence on fossil fuels, as well as to increase the efficiency of vehicle operation (Wu et al., 2015). In support of this, comparative studies based on field measurements show that on average the EVs are more energy efficient than hybrid vehicles and internal combustion engine vehicles (Howey et al., 2011; Lorf et al., 2013). In this context, EVs have received wide attention over the last

* Corresponding author at: Faculty of Engineering, University of Deusto, Avda Universidades, 24, 48007 Bilbao, Spain.

E-mail address: kostas.genikomsakis@deusto.es (K.N. Genikomsakis).

years due to their distinctive advantages (Yao et al., 2013), while main drivers of their market uptake include the government support both on the demand and supply side, the release of new EV models by the automotive industry, as well as the growing interest from the side of the consumers. However, the figures of global EV sales reveal not only that the market size is small, but also that the gradually increasing EV global stock is the result of the adoption in a small number of countries. It is indicative that the share of EVs rose from 0.02% of total passenger cars in 2012 (IEA, 2013) to 0.08% in 2014 (IEA, 2015), with over 95% of the global EV stock accumulated in the sixteen participating countries of the Electric Vehicle Initiative (EVI), indicating that EV cost and uncertainties on performance are among the main barriers to EV worldwide adoption.

Despite the advances in battery technologies, EVs are still characterized by low cruising range (autonomy), a fact that has led to significant research efforts on developing routing applications to compute energy efficient or optimal paths under realistic constraints (Baum et al., 2013, 2014; Schneider et al., 2014; Yang et al., 2015). As a general rule, EV routing algorithms typically assign a representative consumption value (cost) to each segment (arc) of the road network in order to compute energy-optimal paths, while various techniques can be employed to handle negative arc costs due to energy recuperation (Baum et al., 2013). The latter comprises a key feature that contributes to the higher energy efficiency of EVs by using the electric motor to convert the kinetic energy to electrical energy and recharge the battery, for instance, during braking or driving downhill (Wu et al., 2015).

From the modeling perspective, the ability of EVs to recuperate and store energy is often approximated by a constant regeneration factor in the relevant literature of energy consumption models for EVs (Campanari et al., 2009; Li et al., 2015; Muneer et al., 2015; Smith, 2010; Travesset-Baro et al., 2015; Van Sterkenburg et al., 2011), while other published works are based on a speed-dependent regenerative braking factor expressing the percentage of the total braking energy that can be recovered by the motor (Yang et al., 2013; Zhang and Yao, 2015). For the same purpose, speed-dependent recuperation moments and engine's rotational speed are employed by Schellenberg et al. (2014). Moreover, a different approach is presented in the work of Fiori et al. (2016) for the development of the Comprehensive Power-based EV Energy consumption Model (CPEM), where the regenerative energy efficiency is computed as a function of the instantaneous deceleration of the vehicle. However, all the aforementioned models assume a constant value either for the efficiency of the electric motor (regardless of its load) or the energy regeneration factor, or both.

In addition to the energy consumption models for battery EVs reported above, existing vehicle simulation tools that support this type of EVs include: (i) the AVL CRUISE which comprises a software package for vehicle system and driveline analysis based on an object-orientated physical model approach (AVL, 2016), (ii) the AUTONOMIE which combines a driver model, an environment model, an optional vehicle controller, and the vehicle propulsion architecture in a forward-facing simulation approach (ANL, 2016), (iii) the ADvanced VehIcle Simulator (ADVISOR) which combines a backward/forward facing simulation approach (NREL, 2003), and (iv) the Future Automotive Systems Technology Simulator (FASTSim) which is a high-level vehicle powertrain model (NREL, 2014). However, vehicle modeling with these tools is typically a data-intensive process, which requires highly-detailed and potentially confidential manufacturer data with respect to vehicle characteristics as input parameters, while simulation execution is computationally expensive, in particular for routing applications.

The purpose of the present work is to support the algorithmic approaches for energy-efficient routing of EVs developed in the frame of the MOVESMART project, which aims at providing time-dependent route planning and renewable personal mobility services in large-scale urban traffic networks by exploiting a traffic prediction mechanism based on historical and crowd-sourced traffic data (MOVESMART, 2016). In this context, this paper focuses on the development and validation of a battery EV simulation model, which can be combined with pre-defined real-world driving cycles (speed profiles) in order to extract energy consumption factors for various EV configurations under different traffic conditions and road topologies, following a similar approach to the Handbook Emission Factors for Road Transport (HBEFA) that provides fuel consumption and emission factors for different categories and types of conventional vehicles with internal combustion engines (INFRAS, 2015). In the frame of the MOVESMART project, the challenge is to develop a computationally efficient yet accurate energy consumption model that can differentiate between the various EV configurations, serving as the basis for enabling the end user to receive route suggestions optimized for the preferences and EV characteristics defined in the user profile, given the traffic predictions for the state of the road network. This further implies that the focus is on battery EVs used as passenger cars.

To exemplify the intended application, it is pertinent to note that the representation of a route plan in MOVESMART includes position and time of presence information in the form of a sequence of tuples, i.e. <latitude, longitude, time of presence>, as generated by the MOVESMART routing services, given the traffic predictions for the state of the road network provided by the MOVESMART traffic prediction mechanism (note: the integration of the routing services with the traffic prediction mechanism in MOVESMART is clearly out of the scope of the present paper). Then, for a given EV, the estimated energy consumption over a suggested route is calculated as the sum of the products $d_k EC_k$, where d_k (in m) denotes the length of route segment k and EC_k (in W h/m) denotes the EV energy consumption per unit of distance for route segment k that depends on the EV characteristics, road gradient and level of service (in route segment k). Taking into account the area type, road type and speed limit of the route segment k , the level of service is inferred from the average traversal speed (in m/s) in the corresponding route segment k , i.e. $V_{avg,k} = d_k / \Delta Time_of_presence$, where $\Delta Time_of_presence$ (in s) is the difference between the time of presence at the starting points of route segments k and $k + 1$ of a route plan. In this framework, the developed energy consumption model is employed to create a database of EC_k factors for the possible combinations of:

- Vehicle characteristics, such as motor type, motor power, and battery type.
- Road network characteristics and conditions, such as area type (i.e. urban/rural), road type (e.g. motorway/trunk road/distributor/local/access-residential), road speed limit (in increments of 10 km/h), road gradient (ranging from -6% to +6%), and level of service (i.e. free flow/heavy/saturated/stop and go), as represented by the speed profiles of pre-defined driving cycles.

In this direction, the present paper proposes a computationally efficient model to estimate the energy consumption of an EV, based on a high-level representation of its main components, while employing a dynamic approach that combines vehicle speed and motor torque limitations in order to simulate the energy recuperation capability of the EV. In this regard, the proposed simulation model strikes a reasonable balance between model complexity and efficacy of representation, enabling the fast computation of EV consumption factors for various road gradients and given speed profiles representing different driving conditions. Hence, the major contribution of this paper is the development of an energy consumption model for battery EVs that combines the following characteristics: (i) it employs a novel approach that takes into account the electric motor overload to represent the EV performance under highly demanding driving conditions, (ii) it simultaneously considers the dependency of both the electric motor's efficiency and vehicle's energy regeneration capability on the operation conditions, as opposed to the EV energy consumption models reported in the literature, (iii) it comprises a light-weight implementation particularly suitable for routing applications, in contrast to the vehicle simulation tools that are characterized by high model complexity and execution times, (iv) it employs generic technical specification data as input parameters that are typically available on vehicle information leaflets and online sources (e.g., manufacturer's website), avoiding thus the necessity of highly-specific (and potentially confidential) manufacturer data or field measurements for determining the parameters of vehicle components, and (v) it is validated by comparing the results obtained from FASTSim, which is an advanced vehicle powertrain systems analysis tool developed and tested on the basis of real-world data from existing vehicles (Brooker et al., 2015).

More specifically, the contributions of the present paper include not only the methodological approach to represent the dynamics of EV operation in the framework described above, but also the assessment of the developed simulation model in terms of execution time and accuracy using well-established evaluation criteria of model performance over typical driving cycles for future reference. In more concrete terms, the former emphasizes on modeling both normal and overload conditions of EV operation as well as the dependency of the electric motor's efficiency and EV's energy recuperation capability on the motor load and vehicle speed (in sharp contrast to the other relevant energy consumption models in the literature), while the latter facilitates the comparative analysis of model output using standard benchmark datasets. Given that the model development process is based on fundamental principles of physics, it becomes clear that this work builds upon existing knowledge to propose a validated energy consumption model for EVs, introducing simplifying approximations to reduce the computational complexity compared to vehicle simulation tools, while retaining a reasonably detailed modeling level that incorporates the aforementioned motor overload and dynamic energy recuperation features, in order to meet the requirements of route planning applications in general, and MOVESMART project in particular.

The rest of the paper is organized as follows: Section 2 introduces the proposed EV model and the subsequent Section 3 describes the process for its validation. Section 4 presents a comprehensive analysis of the results obtained for specific driving cycles and discusses their significance, while the last section underlines the main conclusions of this work.

2. Methodology

In the frame of the present work, the approach followed to simulate the performance and estimate the energy consumption of EVs combines a generic physics-based vehicle model with the operational characteristics of the main EV components in order to transform the traction power requirements (at wheels) into EV battery power requirements. The proposed simulation model takes also into account the consumption of the EV accessories as well as the losses in the battery, motor and transmission (gear) system, as shown in the high-level representation of the two-way power flow between the main EV components (Fig. 1). In this regard, it is noted that electrical energy is drawn from the battery and transformed to kinetic energy to drive the vehicle, while mechanical energy is transformed to electrical energy during braking or driving downhill (depending on the influence of the hill driving force compared to the other forces that act on the moving vehicle).

2.1. Traction power at wheels

As a starting point, a generic physics-based model provides the theoretical foundation for the estimation of the tractive effort F_{te} (in N) required to overcome the forces opposing to the movement of the vehicle and accelerate it. In particular, the tractive effort refers to the forward driving force which is transmitted to the ground through the wheels in order to propel the vehicle (Larminie and Lowry, 2012), as defined in Eq. (1), where F_{ad} is the aerodynamic drag (in N), F_{rr} is the rolling resistance force (in N), F_{hc} is the hill climbing force (in N), F_{la} is the linear acceleration force of the vehicle (in N), and F_{wa} is the inertia force (in N) of the rotating parts of the vehicle (Travesset-Baro et al., 2015).

$$F_{te} = F_{ad} + F_{rr} + F_{hc} + F_{la} + F_{wa} \quad (1)$$

The aerodynamic drag F_{ad} represents the force that opposes the vehicle's motion through the air, as given in Eq. (2).

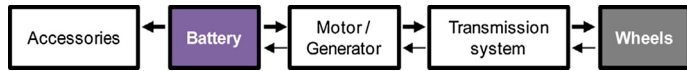


Fig. 1. Power flows in main components of typical EVs.

$$F_{ad} = \frac{1}{2} \rho A C_d u^2 \quad (2)$$

where ρ is the air density (in kg/m³), A is the frontal vehicle area (in m²), C_d is the aerodynamic drag coefficient, and u is the linear vehicle speed (in m/s).

The rolling resistance force F_{rr} is primarily due to the contact of vehicle tires with the road surface, as expressed in Eq. (3).

$$F_{rr} = \mu_{rr} mg \cos \varphi \quad (3)$$

where μ_{rr} is the rolling coefficient, m is the vehicle mass (in kg), g is the acceleration of gravity (in m/s²), and φ is the angle (in rad) of the incline (slope).

The hill climbing force F_{hc} represents the component of the gravity force that acts on a vehicle climbing on a slope, as given in Eq. (4).

$$F_{hc} = mg \sin \varphi \quad (4)$$

According to Newton's second law of motion, the force F_{la} needed to linearly accelerate a vehicle is given by Eq. (5).

$$F_{la} = m\alpha \quad (5)$$

where α is the linear acceleration of the vehicle (in m/s²).

The inertia force F_{oa} of the rotating parts of the vehicle depends on the moment of inertia of the motor. Given that this factor is usually unknown, a common practice is to apply a mass correction factor C_i for the rotational inertia acceleration as in Eq. (6), with a reasonable approximation being 5% of the vehicle mass (Larminie and Lowry, 2012).

$$F_{oa} = C_i m \alpha \quad (6)$$

The total tractive effort F_{te} is positive when the battery provides power to the motor and negative if the motor works as a generator providing power to the battery. The traction power P_{te} (in W) to drive the vehicle at speed u can then be expressed by Eq. (7).

$$P_{te} = F_{te} u \quad (7)$$

2.2. Transmission system

As a general rule, the wheels of a typical EV are not mounted directly on the motor shaft, but instead there is a gear system which transforms the motor torque into appropriate torque at wheels, as shown in Fig. 2.

Assuming that the gear ratio of the transmission system is g_{ratio} , the angular motor speed ω_{motor} (in rad/s) can be calculated by Eq. (8).

$$\omega_{motor} = g_{ratio} \omega_{wheels} = g_{ratio} \frac{u}{r} \quad (8)$$

where ω_{wheels} is the angular speed of the wheel (in rad/s) and r is its radius (in m).

Considering also the gear efficiency n_{gear} of the transmission system, Eq. (9) expresses the mechanical power $P_{motorout}$ (in W) to or from the motor for the cases where traction power is provided to the wheels or energy is recovered (generator mode) respectively, while Eq. (10) gives the motor output torque $T_{motorout}$ (in N m).

$$P_{motorout} = \begin{cases} P_{te} n_{gear}, & P_{te} < 0 \\ P_{te}/n_{gear}, & P_{te} > 0 \end{cases} \quad (9)$$

$$T_{motorout} = \frac{P_{motorout}}{\omega_{motor}} \quad (10)$$

2.3. Motor

Nowadays, there are two types of motors that are widely used in EV applications, namely induction motors (IMs) and permanent magnet brushless dc motors (PM BLDC) (Pellegrino et al., 2012a, 2012b; Yildirim et al. 2014). The former offer low cost, robustness, structure simplicity and operation in any environmental conditions, while the latter have higher power density and efficiency.

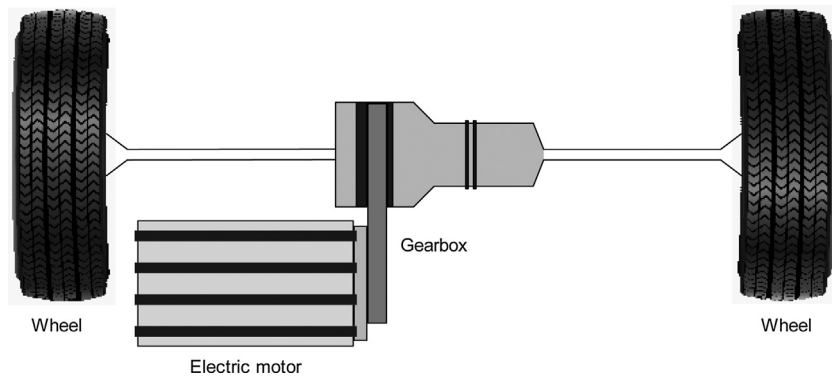


Fig. 2. Simple representation of transmission system connecting the motor shaft with the vehicle wheels.

2.3.1. Efficiency curve

Most electric motors are designed to operate from 50 to 100% of the rated load, having the highest efficiency roughly at 75%. For loads below 50%, the efficiency of the motor decreases dramatically (U.S. Department of Energy, 1997). Fig. 3 presents the part-load efficiency curves of typical electric motors of different rated power.

In the proposed model, the construction of the part-load efficiency curves for the two motor types under study, i.e. induction and synchronous, is based on the efficiency values at 0, 25%, 50%, 75% and 100% of rated load using rational and linear fitting. More specifically, it is assumed that the motor part load-efficiency curve follows the schema in Table 1, where the *mineff* and *maxeff* values are inferred from the fact that the efficiency of an IM typically varies between 88% and 92% and for a BLDC motor from 92% to 95% (Vodovozov et al., 2014).

Using the characteristic points in Table 1 and the efficiency range of each motor type, the load-efficiency curve can be approximated by the piecewise function in Eq. (11).

$$\text{efficiency}(x) = \begin{cases} (\text{cout1}x + \text{cout2})/(x + \text{cout3}), & 0 \leq x < 0.25 \\ \text{dout1}x + \text{dout2}, & 0.25 \leq x < 0.75 \\ \text{eout1}x + \text{eout2}, & x \geq 0.75 \end{cases} \quad (11)$$

where x denotes the mechanical power of the motor P_{motorout} as a fraction of its rated power $P_{\text{motorrated}}$ (in kW), i.e. $x = 0.001|P_{\text{motorout}}|/P_{\text{motorrated}}$.

The coefficients cout1 , cout2 , cout3 , dout1 , dout2 , eout1 , and eout2 are calculated for each motor type using the MATLAB fitting tool and the corresponding efficiency curves are presented in Fig. 4.

At this point, it is worth mentioning that when the electrical machine operates as a generator, the coefficients are different, since the mechanical power is the input and the electric power is the output respectively. Similarly, the load-efficiency curve in this case is also approximated with the piecewise function in Eq. (11), with the difference being that the coefficients are estimated by replacing the points of output power with those of input power. Table 2 shows the values of the relevant coefficients for constructing the load-efficiency curves for each combination of electric machine type and mode of operation.

2.3.2. Motor size

A main characteristic of electric motors is that the efficiency increases with motor size (U.S. Department of Energy, 2014). In the proposed model, the relationship between motor size (in terms of rated power) and efficiency is inferred from the nominal minimum efficiency requirements for electric motors in (European Commission, 2009). Considering that this regulation foresees that electric motors shall comply with the minimum requirements of the IE2 efficiency level (Table 3) from 16 June 2011, the efficiency normalization curve in Fig. 5 is constructed as follows: the average efficiency of IE2 level is calculated for each class of rated power and then it is divided by the maximum average efficiency. The resulting normalization factor *normfactor* represents the value that the motor efficiency in Eq. (11) must be multiplied with in order to take into consideration the motor size in determining its efficiency.

Having determined the motor efficiency curve and the normalization factor, the input power of the motor P_{motorin} (in W) is given in Eq. (12).

$$P_{\text{motorin}} = \begin{cases} P_{\text{motorout}} n_{\text{gen}} \text{normfactor}, & P_{\text{te}} < 0 \\ P_{\text{motorout}} / (n_{\text{mot}} \text{normfactor}), & P_{\text{te}} > 0 \end{cases} \quad (12)$$

where n_{gen} and n_{mot} denote the efficiency of the electric machine when operating as generator and motor respectively, as defined in Eq. (11).

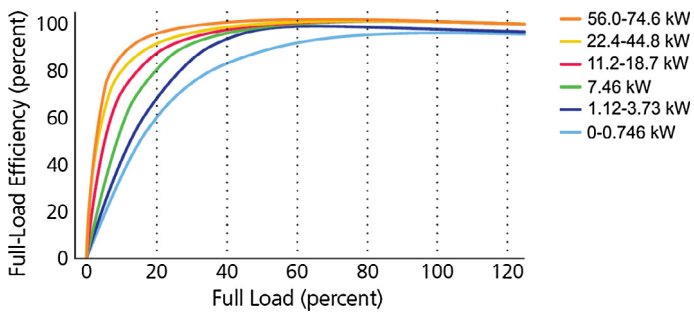


Fig. 3. Typical motor part load-efficiency curves adapted from (Natural Resources Canada, 2004).

Table 1

Nominal motor efficiency at 0%, 25%, 50%, 75% and full rated load.

	Percent load				
	0%	25%	50%	75%	100%
Motor efficiency	0	mineff	0.98 * maxeff	maxeff	0.98 * maxeff

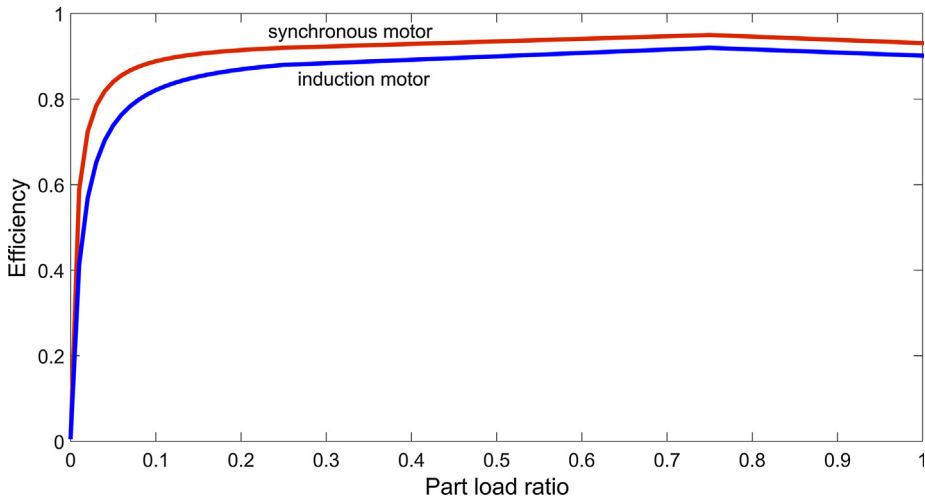


Fig. 4. Part load-efficiency curve of the synchronous (red color) and the induction motor (blue color) of the proposed model. (For interpretation of the references to color in this figure legend, the reader is referred to the web version of this article.)

Table 2

Coefficients of piecewise function for determining the efficiency in motor/generator mode.

Coefficient	Induction electric machine		Synchronous electric machine	
	Motor mode	Generator mode	Motor mode	Generator mode
cout1	0.924300	0.925473	0.942269	0.942545
cout2	0.000127	0.000148	0.000061	0.000067
cout3	0.012730	0.014849	0.006118	0.006732
dout1	0.080000	0.075312	0.060000	0.057945
dout2	0.860000	0.858605	0.905000	0.904254
eout1	-0.073600	-0.062602	-0.076000	-0.066751
eout2	0.975200	0.971034	1.007000	1.002698

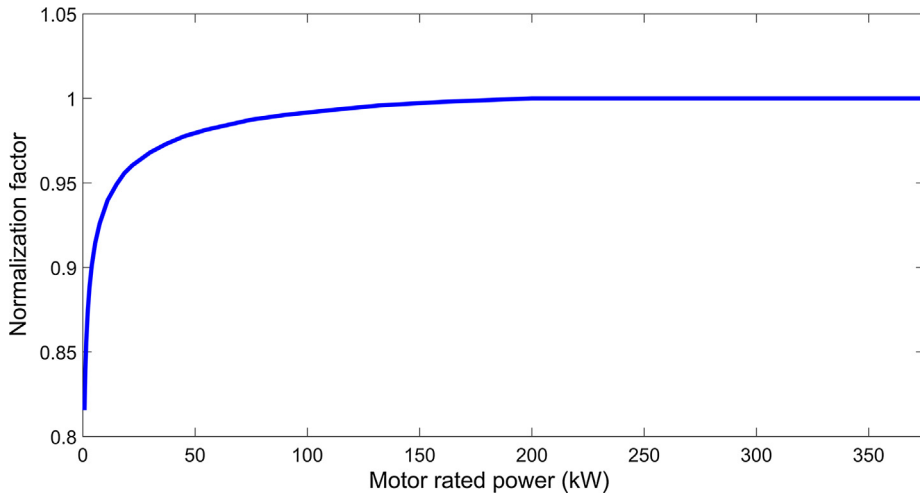
2.3.3. Motor drive characteristics

The desired motor drive performance is divided into two regions, namely the constant-torque region and the constant-power region. For angular speeds below the base value ω_{base} (in rad/s), the motor drive must provide high torque in order to achieve the gradeability and acceleration requirements of the vehicle. For values beyond the base speed and up to the

Table 3

Nominal minimum efficiency requirements for IE2 efficiency level motors [retrieved from (European Commission, 2009)] and proposed efficiency normalization factor based on rated output power.

Rated output power (kW)	Number of poles			Average	Normalization factor
	2 poles	4 poles	6 poles		
0.75	77.4	79.6	75.9	77.63	0.817
1.1	79.6	81.4	78.1	79.70	0.839
1.5	81.3	82.8	79.8	81.30	0.855
2.2	83.2	84.3	81.8	83.10	0.874
3	84.6	85.5	83.3	84.47	0.889
4	85.8	86.6	84.6	85.67	0.901
5.5	87.0	87.7	86.0	86.90	0.914
7.5	88.1	88.7	87.2	88.00	0.926
11	89.4	89.8	88.7	89.30	0.940
15	90.3	90.6	89.7	90.20	0.949
18.5	90.9	91.2	90.4	90.83	0.956
22	91.3	91.6	90.9	91.27	0.960
30	92.0	92.3	91.7	92.00	0.968
37	92.5	92.7	92.2	92.47	0.973
45	92.9	93.1	92.7	92.90	0.978
55	93.2	93.5	93.1	93.27	0.981
75	93.8	94.0	93.7	93.83	0.987
90	94.1	94.2	94.0	94.10	0.990
110	94.3	94.5	94.3	94.37	0.993
132	94.6	94.7	94.6	94.63	0.996
160	94.8	94.9	94.8	94.83	0.998
200–375	95.0	95.1	95.0	95.03	1.000

**Fig. 5.** Normalization factor curve.

maximum motor speed ω_{max} (in rad/s), EVs require high power (Vagati et al., 2010). The desired motor drive characteristics are expressed in Eq. (13) and depicted in Fig. 6. Indicative values of the ratio between the base and maximum motor speed are 1:5 and 1:2.25 for induction and BLDC motors respectively (Rahman and Ehsani, 1996; Yildirim et al., 2014).

$$T_{max}(\omega_{motor}) = \begin{cases} T_{max}, & \omega_{motor} \leqslant \omega_{base} \\ P_{max}/\omega_{motor}, & \omega_{base} < \omega_{motor} \leqslant \omega_{max} \end{cases} \quad (13)$$

where T_{max} and P_{max} denote the maximum nominal torque (in N m) and power (in W) of the motor respectively.

In practice, an electric motor can safely operate under overload (torque and power) conditions for a couple of minutes in order to respond to the requirements for vehicle acceleration at any speed (Vagati et al., 2010). As an indicative example, Pellegrino et al. (2012b) consider two different types of PM motors for EV applications with overload torque percentage of 23% and 82% respectively. For the purposes of the proposed model, if the motor's calculated torque (according to the traction power requirements) is greater than the maximum torque specified by the torque-speed characteristic curve, it is assumed that the motor drive can operate under overload conditions for 15 s (as a conservative approach) to deliver

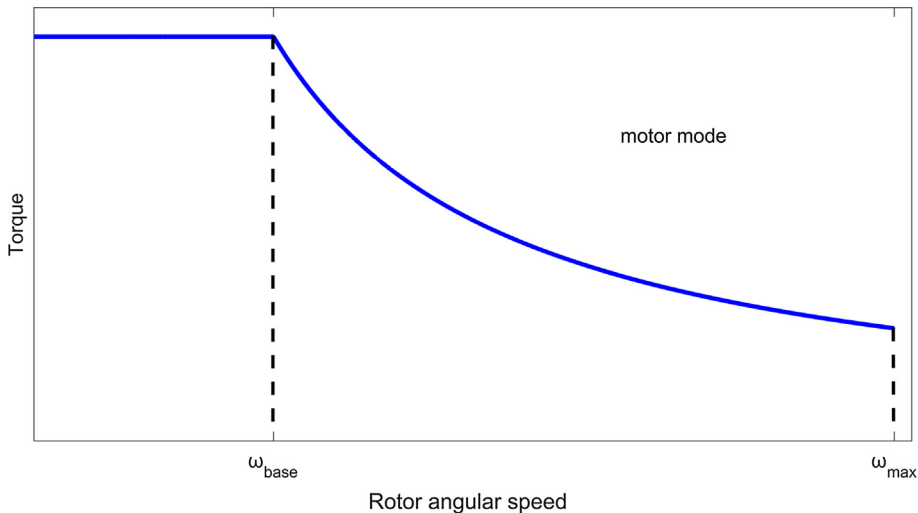


Fig. 6. Desired motor drive characteristics.

additional torque up to a maximum of 52.5% of nominal torque, enabling an EV to complete highly demanding route sections with respect to motor torque.

2.3.4. Regenerative braking

Admittedly, a key feature of an EV is its ability to recuperate energy during regenerative braking, where the motor inverts its operation and acts as a generator, converting the kinetic energy of the vehicle to electric energy, which is stored back to the EV battery. It follows that this process is subject to some restrictions, and thus its modeling requires a number of assumptions as described below.

Firstly, it is assumed that the torque-speed curve in generator mode is symmetric to that in motor mode, implying that the torque takes negative values during regenerative braking, as shown in Fig. 7. Moreover, the operation of the mechanical and regenerative braking systems is complementary due to the maximum torque limitation of the electrical machine and the maximum state of charge (SoC) of the battery (Yeo et al., 2004). Specifically, when the braking torque is lower than or equal to the maximum generator torque (points A and B respectively in Fig. 7), only the regenerative brake is applied. On the contrary, if the braking torque exceeds the torque limit (point C in Fig. 7), the generator operates at the maximum torque point (P_{regen}) and the rest of the power (P_{mech}) is wasted as heat due to the mechanical braking (Gao and Ehsani, 2010).

In addition, the regenerative braking system produces no braking force at low vehicle speeds (Larminie and Lowry, 2012), due to low available torque conditions, and thus the braking mechanical system is solely responsible for the vehicle to come to a standstill (Spichartz et al., 2014). To simulate this operation, the proposed model considers a speed-dependent regeneration factor $regenfactor(u)$, which expresses the fraction of available (regenerative) braking power that can be practically recuperated as a function of vehicle speed u . In particular, there is a threshold of vehicle speed u_1 (in m/s) that should be overcome in order for the electrical machine to regenerate energy (Yeo et al., 2004), while the EV reaches its maximum regeneration capability for speeds above the threshold speed u_2 (in m/s). For speeds between u_1 and u_2 , it is assumed that the percentage of recoverable braking power increases linearly with vehicle speed up to the point of maximum regeneration capability, as shown in Fig. 8. It is noted though that the recoverable braking power is subject to the torque limitation (Fig. 7) for all the aforementioned cases. Taking into account the above, Eq. (12) becomes:

$$P_{motorin} = \begin{cases} P_{motorout} regenfactor(u) n_{gen} normfactor, & P_{te} < 0 \\ P_{motorout} / (n_{mot} normfactor), & P_{te} > 0 \end{cases} \quad (14)$$

2.3.5. Battery

In the frame of this work, the energy or power losses during battery discharging (conversion of chemical energy into electric) and charging (conversion of electric energy into chemical) are expressed through its roundtrip efficiency factor. Table 4 shows the relevant efficiencies of typical battery types used in electromobility applications (Ehsani et al., 2010; Piller et al., 2001; Qian et al., 2011). In this context, the power flow of the battery in each time instance is expressed in Eq. (15).

$$P_{total} = \begin{cases} P_{batteryout} \sqrt{RTE}, & \text{battery charging } (P_{batteryout} < 0) \\ P_{batteryout} / \sqrt{RTE}, & \text{battery discharging } (P_{batteryout} > 0) \end{cases} \quad (15)$$

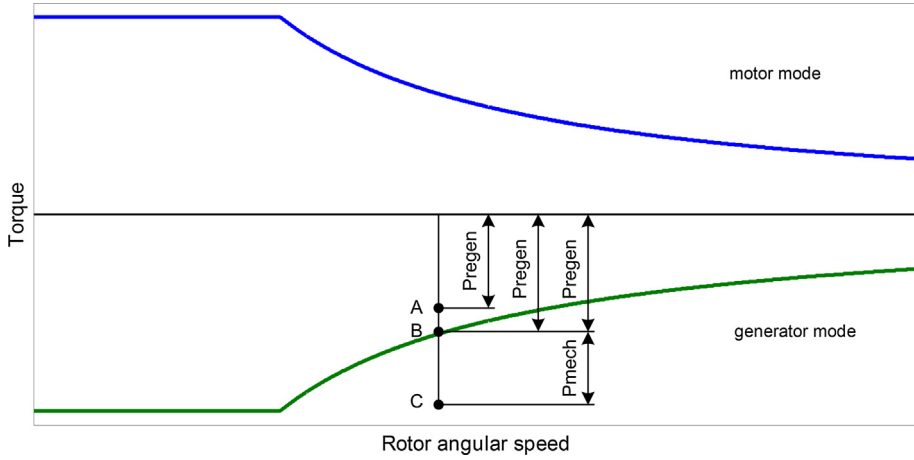


Fig. 7. Maximum motor braking torque curve.

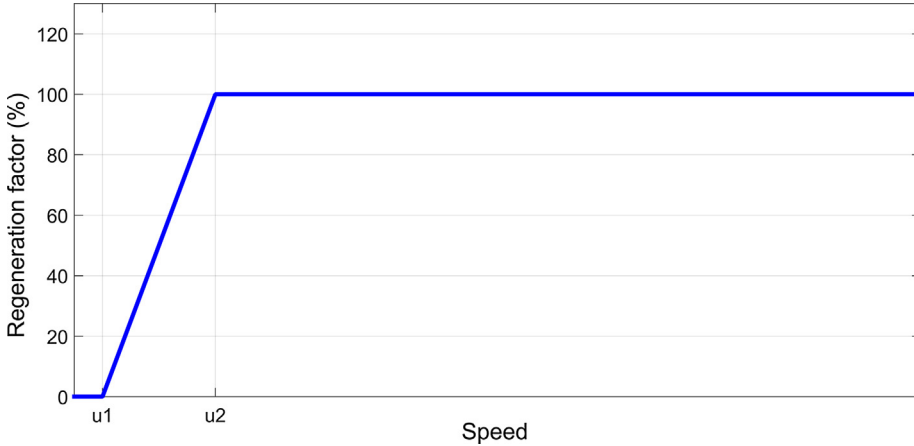


Fig. 8. Speed-dependent regeneration factor.

Table 4

Energy efficiency of typical battery types for EVs [retrieved from (Ehsani et al., 2010)].

Battery type	Energy efficiency
Lead acid	>80%
NiCad	75%
NiMH	70%
Lilon	>95%

where P_{total} (in W) and RTE denote the total power and round trip efficiency of the EV battery respectively, while $P_{batteryout}$ (in W) is the electric output of the battery to provide power P_{ac} (in W) to the accessories (auxiliary loads) of the EV, and supply the motor with electric power ($P_{motorin} > 0$) or receive electric power from the generator ($P_{motorin} < 0$), as given in Eq. (16).

$$P_{batteryout} = P_{motorin} + P_{ac} \quad (16)$$

The cumulative energy consumption $E(t)$ in each time instance t can be computed by Eq. (17).

$$E(t) = E(t-1) + \int_{t-1}^t P_{total}(\tau) d\tau \quad (17)$$

Combining Eqs. (9), (11) and (14)–(17), the estimation of cumulative energy consumption $E(t)$ (in W h) can be analytically expressed by the following equation:

$$E(t) = \begin{cases} E(t-1) + [P_{te}(t)n_{gear}n_{gen}\left(\frac{0.001|P_{motorout}(t)|}{P_{motorrated}}\right)\text{regenfactor}(u(t))\text{normfactor} + P_{ac}]\Delta t/\sqrt{RTE}, & P_{te} < 0 \text{ and } P_{batteryout} < 0 \\ E(t-1) + [P_{te}(t)n_{gear}n_{gen}\left(\frac{0.001|P_{motorout}(t)|}{P_{motorrated}}\right)\text{regenfactor}(u(t))\text{normfactor} + P_{ac}]\Delta t/\sqrt{RTE}, & P_{te} < 0 \text{ and } P_{batteryout} > 0 \\ E(t-1) + \left[\frac{P_{te}(t)}{n_{gear}n_{mot}\left(\frac{0.001|P_{motorout}(t)|}{P_{motorrated}}\right)\text{normfactor}} + P_{ac} \right] \Delta t/\sqrt{RTE}, & P_{te} > 0 \end{cases} \quad (18)$$

where Δt is 1/3600 h. The first sub-function represents the case where the regenerated energy exceeds the consumption of the accessories and the excess of energy is stored to the battery, the second sub-function represents the case where the regenerated energy is not sufficient to cover the consumption of the accessories and thus energy is drawn from the battery, while the third sub-function represents the case where no energy regeneration occurs and energy is drawn from the battery to provide the power required to move the vehicle and cover the consumption of the accessories.

3. Model validation

In this work, the proposed simulation model is validated by comparing its output with the results obtained from FASTSim developed by the U.S. National Renewable Energy Laboratory (NREL). FASTSim is an automotive systems simulation tool capable of estimating vehicle efficiency, cost, performance, and battery life, while its output has been validated with test data from a list of different vehicles, providing thus high accuracy and reliability to the underlying model (Brooker et al., 2015). In this context, the simulation results obtained from the proposed model and FASTSim, with respect to energy consumption over typical driving cycles representing different driving conditions, are compared using well established measures of accuracy.

3.1. Driving cycles

This subsection presents the driving cycles employed to represent the profile of vehicle speed in order to assess the performance of the proposed EV model. Specifically:

- *Urban Dynamometer Driving Schedule (UDDS)*: The UDDS cycle (Fig. 9a), also known as US FTP-72 (Federal Test Procedure), has been developed by the United States Environmental Protection Agency (US EPA) and simulates city driving conditions with frequent stops by car. The duration of the cycle is 1369 s and represents a route with distance of almost 12 km and average speed of 31.6 km/h (Barlow et al., 2009).
- *Highway Fuel Economy Test (HWFET)*: The HWFET cycle (Fig. 9b) is a chassis dynamometer driving schedule developed by US EPA to simulate the highway driving conditions for light-duty vehicles. The duration of the cycle is 765 s, representing a route with distance of 16.5 km and average speed of 77.7 km/h (Barlow et al., 2009).
- *JP 10 Mode cycle*: The JP 10 Mode driving schedule (Fig. 9c) was used for type approval purposes of light-duty vehicles in Japan and comprises a component of the newer JP 10-15 Mode cycle. The duration of the JP 10 Mode cycle is 135 s, representing a 0.663 km route with an average speed of 17.7 km/h (Barlow et al., 2009).
- *JP 15 Mode cycle*: The JP 15 Mode driving schedule (Fig. 9d) is a component of the legislative cycle JP 10-15 Mode for light-duty vehicles. The duration of the JP 15 Mode cycle is 231 s and represents a route of 2.17 km with an average speed of 33.88 km/h (U.S. Environmental Protection Agency, 2013).
- *LA92-Unified*: The LA92-Unified cycle (Fig. 9e), also referred to as California Unified Cycle (UC), is a dynamometer driving test for light-duty vehicles developed by the California Air Resources Board. It represents aggressive city-driving conditions and its characteristic parameters include duration of 1435 s, distance of 15.8 km and average speed of 39.6 km/h (Barlow et al., 2009).
- *LA92-Short*: The LA92-Short cycle (Fig. 9f) consists of the first 969 s of the LA92-Unified with an average speed of 41.75 km/h and a total distance of 11.25 km (U.S. Environmental Protection Agency, 2013).
- *New York City Cycle (NYCC)*: The NYCC driving schedule (Fig. 9g) is a dynamometer test for light-duty vehicles, developed by US EPA, and represents low speed stop-and-go urban driving conditions. The characteristic parameters of this cycle include duration of 598 s, distance of 1.9 km and average speed of 11.5 km/h (Barlow et al., 2009).
- *US06 Supplemental Federal Test Procedure (SFTP)*: The SFTP cycle (Fig. 9h), also referred to as US06, was developed by US EPA and simulates a high acceleration aggressive highway driving schedule for light-duty vehicles. The duration of this cycle is 596 s, representing a 12.89 km route with an average speed of 77.9 km/h (Barlow et al., 2009).
- *New European Driving Cycle (NEDC)*: The NEDC dynamometer test (Fig. 9i) is a driving schedule for type approval purposes of passenger cars in Europe. It consists of four sub-cycles simulating city driving and an additional sub-cycle for highway driving conditions. The duration of the total cycle is 1180 s, representing an 11 km route with an average speed of 33.6 km/h (Barlow et al., 2009).

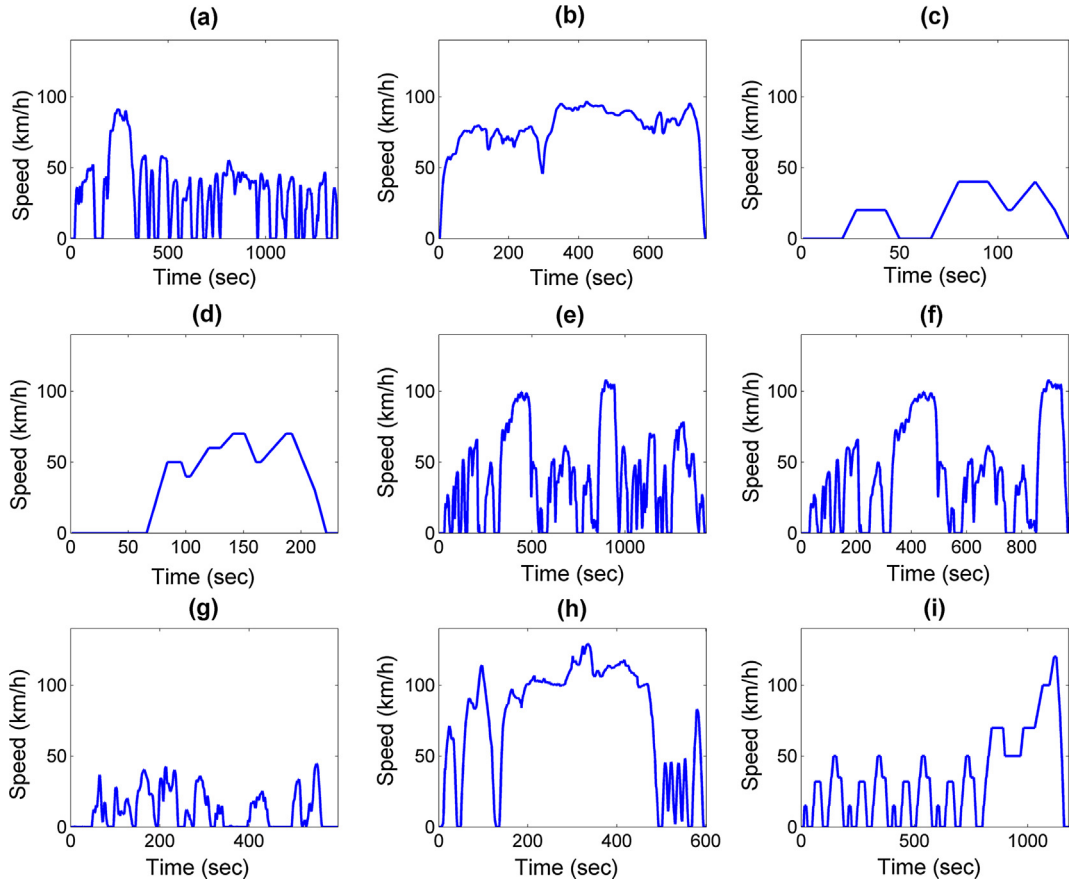


Fig. 9. Typical driving cycles: (a) UDDS, (b) HWFET, (c) JP 10 Mode, (d) JP 15 Mode, (e) LA92-Unified, (f) LA92-Short, (g) NYCC, (h) SFTP, and (i) NEDC.

3.2. Model parameters and characteristics of test vehicle

The Nissan Leaf model is used for the comparison between the simulation results of the proposed model and the ones of FASTSim. The main model parameters and technical specifications of the vehicle are shown in Table 5 ([Carsales.com.au, 2015](#)). To the extent possible, the same values with FASTSim are assumed for the main vehicle parameters (e.g. total mass, drag coefficient, frontal area, rolling coefficient, gear efficiency and power consumption of accessories) in order to establish a common basis for the comparison of the results. Moreover, the values of threshold speeds u_1 and u_2 are devised as parameters of the speed-dependent regeneration factor (Fig. 8) to approximate the sigmoid function employed in FASTSim for the same purpose.

3.3. Simulation results and validation

Figs. 10–18 depict the simulation results obtained from the proposed model (blue¹ color) and FASTSim (red color) with respect to cumulative energy consumption and battery output power for each driving cycle in Section 3.1, considering 0% road gradient as well as initial depth of discharge equal to 6% of the EV battery energy (24 kWh) in alignment to the initial conditions in FASTSim. This assumption corresponds to a value of $0.06 * 24 = 1.44$ kWh as a starting point of the calculations of the cumulative energy consumption, i.e. $E(0)$, in Eqs. (17) and (18). At a first glance, these figures confirm qualitatively that there is good correspondence between the results of the two approaches in each case, despite the fact that the employed driving cycles differ not only on the time (in absolute and percentage terms) representing each operating mode (cruising, accelerating, decelerating, and idling), but also on other kinematic parameters, such as maximum, average, and standard deviation of vehicle speed and acceleration/deceleration rate ([Barlow et al., 2009](#)). A closer examination of the cumulative energy consumption plots indicates that only small differences are observed, mostly on the speed profiles (cycles) representing city driving conditions with frequent

¹ For interpretation of color in Figs. 10–18, the reader is referred to the web version of this article.

Table 5
Model parameters and technical specifications of test vehicle.

Parameter	Value
Acceleration of gravity	9.80665 m/s ²
Air density	1.25 kg/m ³
Battery energy	24 kW h
Battery round trip efficiency	0.95
Battery type	Lithium
Drag coefficient	0.29
Frontal area	2.19 m ²
Gear efficiency	0.97
Gear ratio	8.2
Mass correction factor	0.05
Maximum motor power	80 kW @2730–9800 rpm
Maximum motor torque	280 N m @0–2730 rpm
Motor type	Induction
Power consumption of accessories	300 W
Rolling coefficient	0.008
Threshold speed u_1	1.39 m/s (5 km/h)
Threshold speed u_2	4.72 m/s (17 km/h)
Tire radius	0.316 m
Vehicle + driver mass	1663 kg

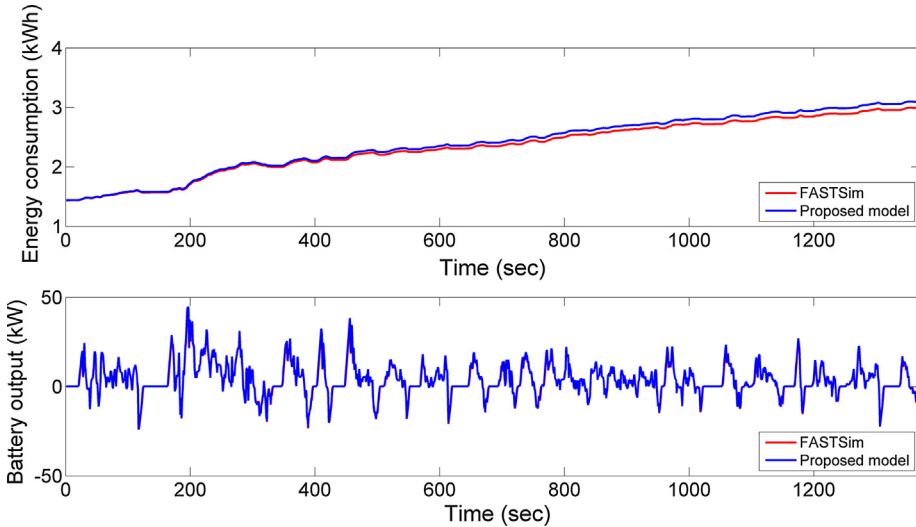


Fig. 10. Cumulative energy consumption and battery output over UDDS.

accelerations and/or varying acceleration rate (e.g. UDDS, LA92-Unified, LA92-Short, and NYCC), or highway driving conditions with stops (e.g. SFTP). In particular, the corresponding curves of cumulative energy consumption (obtained by the proposed model and FASTSim) present slight deviations or even coincide in the cases of JP 10 Mode, JP 15 Mode, and NEDC, which are characterized by phases of constant speed (cruising) and periods of rather steady accelerations, as well as in the case of the HWFET driving cycle that represents highway driving conditions without intermediate stops (note: the scale of Figs. 12, 13 and 16 is different with that of Figs. 10, 11, 14, 15, 17 and 18). Moreover, the relevant figures show that the proposed model systematically overestimates the EV energy consumption compared to that of FASTSim. An alternative interpretation of this observation is that the proposed model follows a more conservative approach in its calculations, and thus it is on the safe side when estimating energy consumption, for instance in an EV routing application. Regarding the instantaneous battery power plots, the results of the proposed model follow the output of FASTSim with high accuracy, implying that its dynamic response is also reliable, even under aggressive driving cycles.

At this point, it is important to note that the differences observed in Figs. 10–18 between the simulation results obtained with the proposed model and FASTSim are due to the different modeling approaches followed in each case. Specifically, the proposed model:

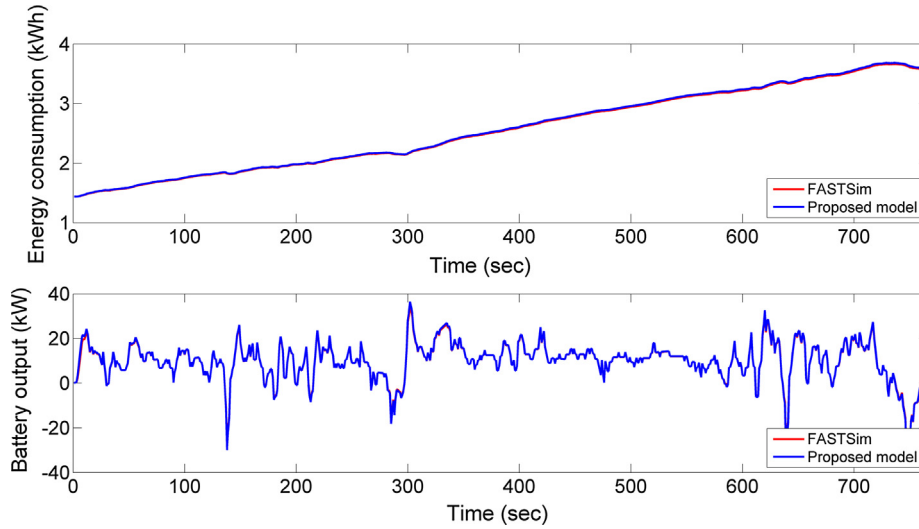


Fig. 11. Cumulative energy consumption and battery output over HWFET.

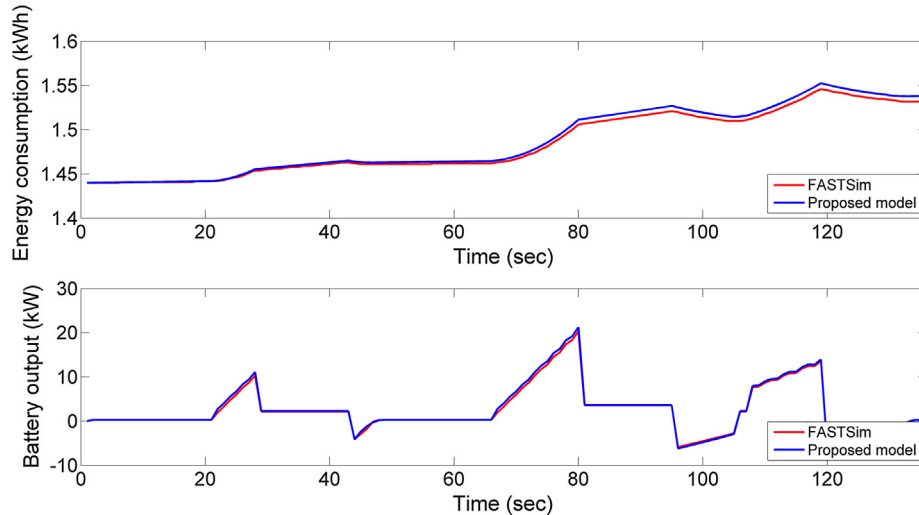


Fig. 12. Cumulative energy consumption and battery output over JP 10 Mode.

- Employs generic technical specification data to represent the vehicle components, in contrast to FASTSim that requires more detailed vehicle data as input parameters, e.g. vehicle center of gravity, drive axle weight fraction, motor time to full power, wheel inertia and mass of each component. As an indicative example, the proposed model assumes a mass correction factor of 5% for the rotational inertia acceleration in Eq. (6), whereas FASTSim calculates the wheel inertia force as a function of the wheel inertia parameter.
- Considers that the electric motor can operate under overload conditions in order to overcome the demanding parts of a driving cycle where the power (or torque) requirements exceed the motor nominal specifications, as opposed to the logic behind FASTSim that compares the desired traction power with the maximum available traction power in every time step and adjusts the vehicle speed (if needed) to make the driving cycle feasible, in which case a third degree polynomial equation is solved to calculate the new speed value.
- Approximates the motor efficiency curve with a piecewise function consisting of a rational segment (where both numerator and the denominator are first degree polynomials) and two linear ones, whereas FASTSim employs a more complex approach based on fourth degree polynomial functions for the same purpose.
- Assumes a linear piecewise function as a reasonable approximation of the sigmoid function used in FASTSim for the speed-dependent regeneration factor.

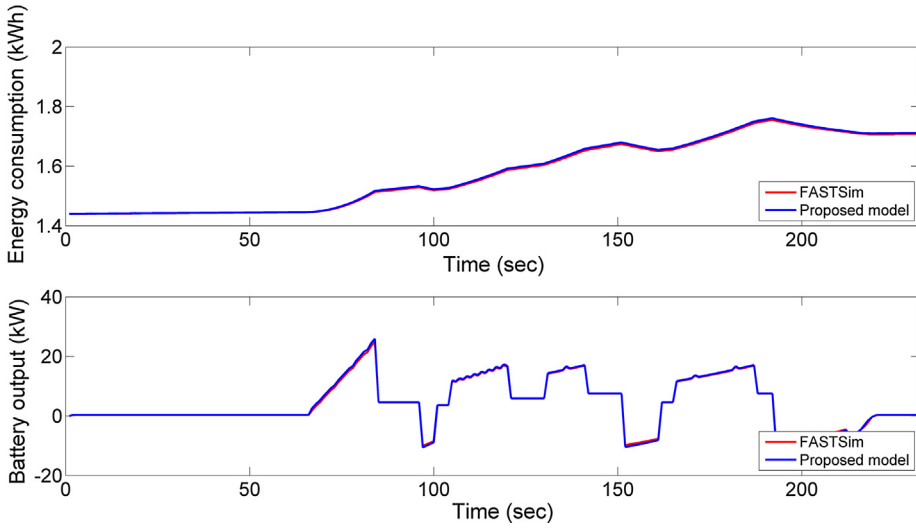


Fig. 13. Cumulative energy consumption and battery output over JP 15 Mode.

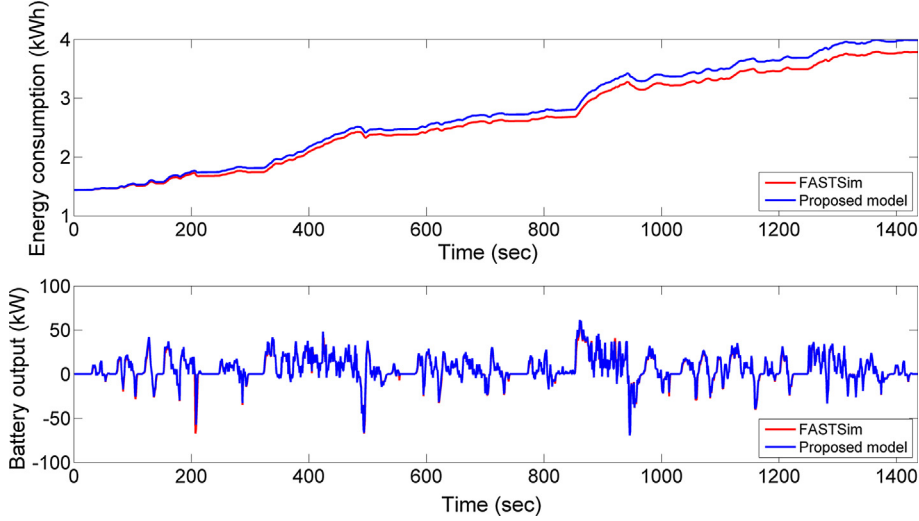


Fig. 14. Cumulative energy consumption and battery output over LA92-Unified.

To quantitatively validate the EV model presented in this work, three typical statistical error indicators are employed, namely the mean absolute error (MAE), the mean squared error (MSE) and the mean absolute percentage error (MAPE), defined in Eqs. (19)–(21) respectively. In this context, Table 6 shows the final energy consumption (net value excluding the initial battery discharge) for each one of the nine driving cycles, as estimated by the EV consumption model proposed here and FASTSim, along with the corresponding values on these well-established evaluation criteria of model performance.

$$MAE = \frac{1}{n} \sum_{i=1}^n |\hat{E}_i - E_i| \quad (19)$$

$$MSE = \frac{1}{n} \sum_{i=1}^n (\hat{E}_i - E_i)^2 \quad (20)$$

$$MAPE = \frac{1}{n} \sum_{i=1}^n \left| \frac{\hat{E}_i - E_i}{E_i} \right| \quad (21)$$

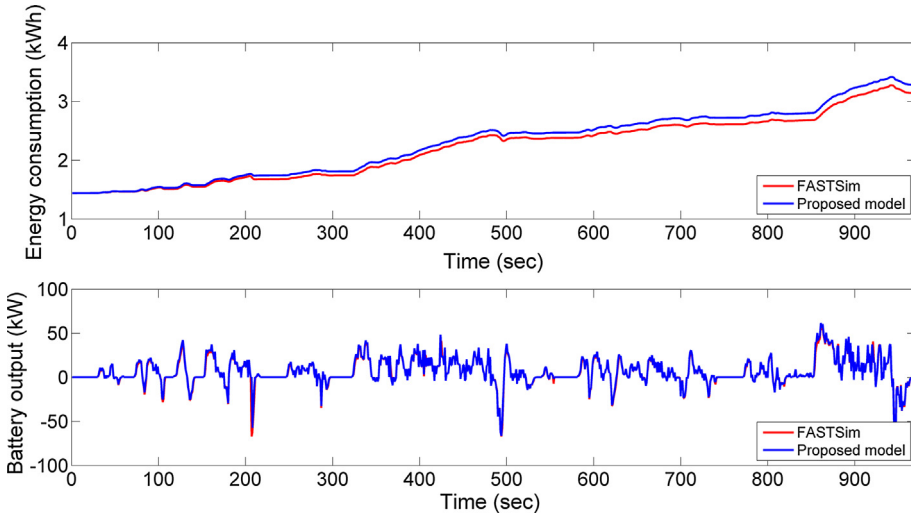


Fig. 15. Cumulative energy consumption and battery output over LA92-Short.

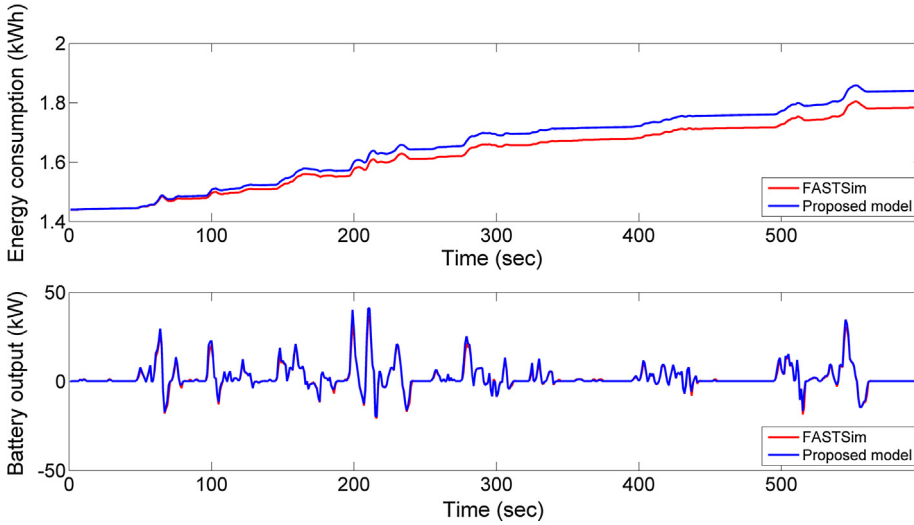


Fig. 16. Cumulative energy consumption and battery output over NYCC.

where \hat{E}_i is the estimated cumulative energy consumption by the proposed model, E_i is the cumulative energy consumption by FASTSim and n is the number of data samples. Particularly, n represents the total time (in s) of a driving cycle, given that the calculations are executed for each second i of the simulation.

The comparative results in Table 6 show that the proposed model simulates the energy consumption of the test vehicle for all the driving cycles under study with sufficient accuracy, given that the values of the MAPE criterion are roughly less than 4%, while the average MAE over the one driving cycles is less than 45 W h. Specifically, the maximum values on the statistical error indicators are observed in the LA92-Unified and LA92-Short driving cycles, which are highly aggressive with fewer stops per kilometer and less idle time. On the contrary, MAPE values below 0.5% are observed in HWFET, JP 10 Mode and JP 15 Mode, which represent smooth driving cycles without high accelerations and high speed variances. For the rest driving cycles, namely UDDS, NYCC, SFTP and NEDC, the values on the measures of error confirm that the proposed model is able to respond accurately in different driving conditions. At this point, it is noted that Fiori et al. (2016) report that the results of the CPEM model on six driving cycles indicate that the energy consumption is accurately estimated with an average error of 5.86% compared to empirical data for the Nissan Leaf as test vehicle. In particular, errors of 16.11%, 0.38%, 8.19%, and -5.35% are presented for the energy consumption (per unit of distance) with the driving cycles UDDS, HWFET, SFTP, and NEDC respectively. In support of the accuracy of the proposed model in the present paper, the corresponding percentage errors of the estimated final energy consumption for these driving cycles are 6.80%, 0.98%, 7.00%, and 3.27% respectively, compared to FASTSim (based on the results shown in Table 6).

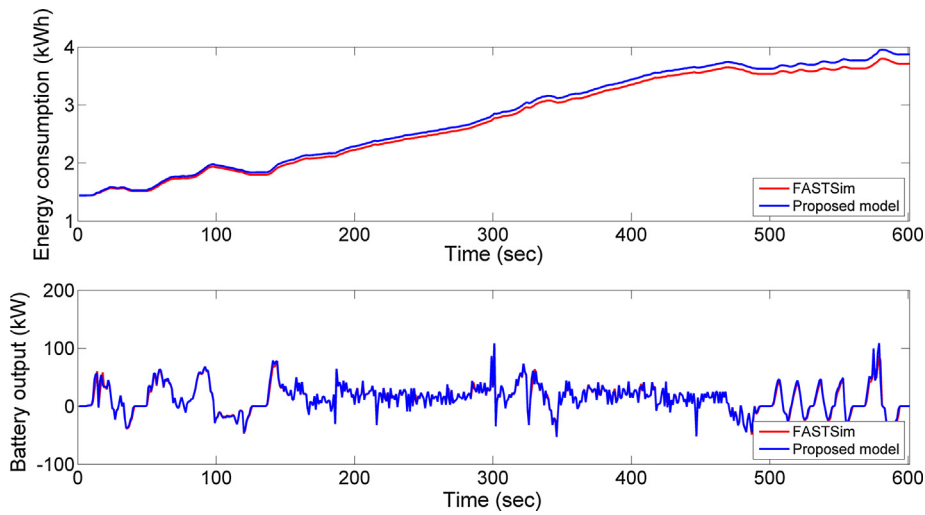


Fig. 17. Cumulative energy consumption and battery output over SFTP.

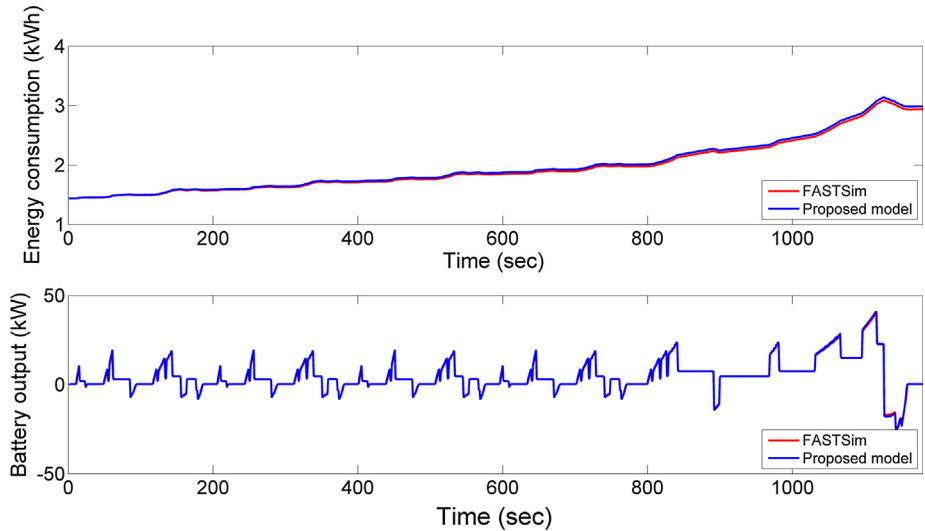


Fig. 18. Cumulative energy consumption and battery output over NEDC.

Table 6

Comparative results on energy consumption over characteristic driving cycles and computation time.

Driving cycle	Proposed model (kW h)	FASTSim (kW h)	MAE (kW h)	MSE (kW h ²)	MAPE (%)	Computation time (s)
Urban Dynamometer Driving Schedule	1.648	1.543	0.05408	0.003862	2.13	0.0286
Highway Fuel Economy Test	2.164	2.143	0.01277	0.000189	0.48	0.0164
JP 10 Mode cycle	0.098	0.093	0.00338	0.000016	0.22	0.0028
JP 15 Mode cycle	0.271	0.268	0.00319	0.000015	0.20	0.0047
LA92-Unified	2.549	2.342	0.11471	0.016684	4.02	0.0302
LA92-Short	1.849	1.707	0.08176	0.008346	3.45	0.0203
New York City Cycle	0.400	0.344	0.03104	0.001254	1.85	0.0121
US06 Supplemental Federal Test Procedure	2.430	2.271	0.07289	0.006527	2.53	0.0128
New European Driving Cycle	1.547	1.498	0.02636	0.000901	1.26	0.0239

Table 6 also shows the average elapsed CPU time to perform each one of the driving cycles with the implementation of the proposed model in MATLAB, where each driving cycle was executed 60 times using a laptop computer with Intel(R) Core(TM) i7-5500U CPU @ 2.40 GHz processor and 8 GB of RAM. A careful examination of results reveals that the computation time is of the order of few tens of milliseconds, confirming that the proposed approach is computationally inexpensive and thus is particularly suitable for the fast extraction of energy consumption factors for EVs and/or computation of trip energy consumption of EVs in real-time. As a side observation, it is noted that there is a linear relationship between CPU time and driving cycle duration.

4. Results and discussion

Figs. 19 and 20 present the simulation results of the test vehicle obtained from the proposed model for different road gradients, ranging from -6% to 6% , over the LA92-Short and SFTP driving cycles respectively (assuming 0% initial depth of discharge for the EV battery). As expected, the difference in the cumulative energy consumption of the EV for the road gradients under study gradually increases over the course of the driving cycles due to the effect of the hill climbing force. A close examination of the simulation results shows that the EV completes both driving cycles with negative cumulative energy consumption for road gradients of -4% or less, implying that there is excess of energy recuperated and stored back to the battery despite the forces opposing to the vehicle movement and the consumption of its accessories (assumed equal to 300 W). For road gradients from -3% to -1% , energy is drawn from the battery in order to provide the required traction power to complete the driving cycles and supply the vehicle accessories, despite the effect of the hill climbing force.

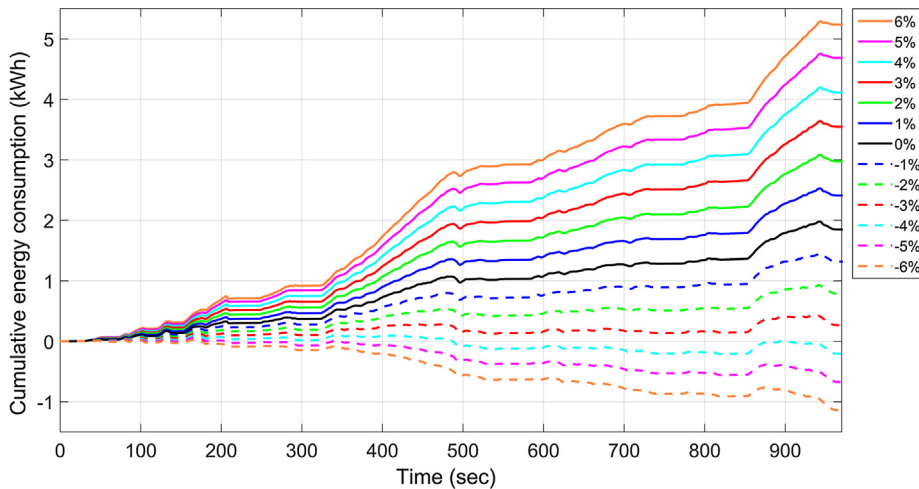


Fig. 19. Cumulative energy consumption for different road gradients over LA92-Short.

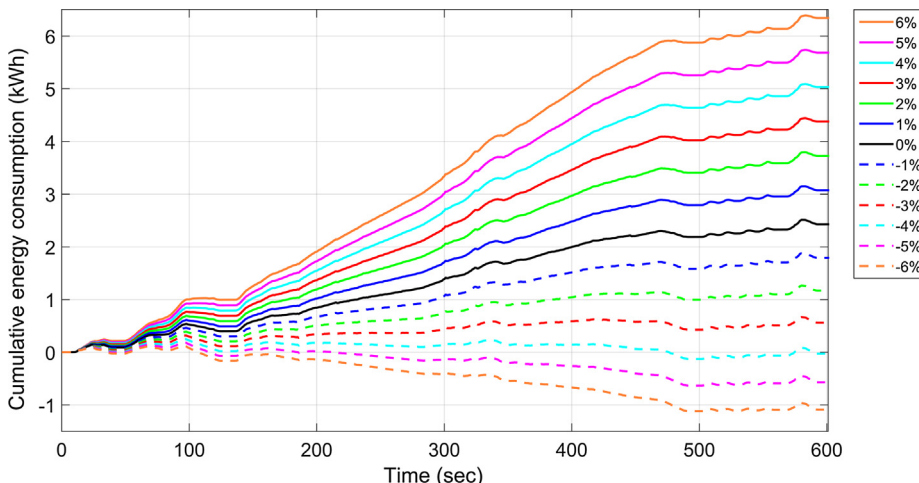


Fig. 20. Cumulative energy consumption for different road gradients over SFTP.

In this context, the capability of the EV to recuperate energy under certain conditions is indicated by the negative gradients in the cumulative energy consumption curves. As an example, for the time period of 400–480 s in Fig. 19, the derivative of cumulative energy consumption is positive between road gradients of -3% and 6% , thus energy is drawn from the battery, whereas between -4% and -6% energy is stored to the battery.

Figs. 19 and 20 also indicate the effect of vehicle speed on the energy consumption rate with respect to the different road gradients. As illustrated by the energy consumption plots for positive road slope in the LA92-Short cycle (Fig. 19), the curve gradients are higher in the time period of 400–500 s compared to those of the period 500–600 s, meaning that the motor absorbs more energy for the same amount of time. On the other hand, there are less variations of the consumption rate in the SFTP cycle, since it consists mainly of a high speed zone period and the total energy consumption increases almost steadily from 150 to 500 s, as seen in Fig. 20.

Fig. 21 depicts the values of the motor torque during the simulation of the SFTP cycle for different road slopes. As also expected, the motor torque increases as the road slope increases from -6% to 6% . However, there are instances where the motor reaches a torque value greater than the nominal one in order to achieve the desired speed (according to the driving cycle profile), a fact that exemplifies the overload torque feature of the proposed model.

It becomes apparent that the frequency of motor overload increases with the road slope, reaching the peak value of 22 times for road gradient of 6% during the simulation of the SFTP cycle, as shown in Fig. 22. Moreover, it is worth noting that the motor needs to be overloaded not only for positive but also negative road gradients. Specifically, motor overload occurs for road gradients from -1% to -4% due to the aggressive nature of the driving cycle, characterized by relatively high speed values, which increase the aerodynamic drag force, and high acceleration driving conditions. For road gradients between -5% and -6% , the motor operates normally and its torque takes values below the maximum torque curve.

For negative torque values, the electric machine operates as a generator returning energy back to the battery as already pointed out. Comparing the absolute torque values of the two operation modes of the electric machine, it is evident that more force is needed for propulsion than for regeneration in both constant torque and constant power regions. Nevertheless, there are two times during the simulation of road gradient -6% and one time of -5% that the machine receives more torque

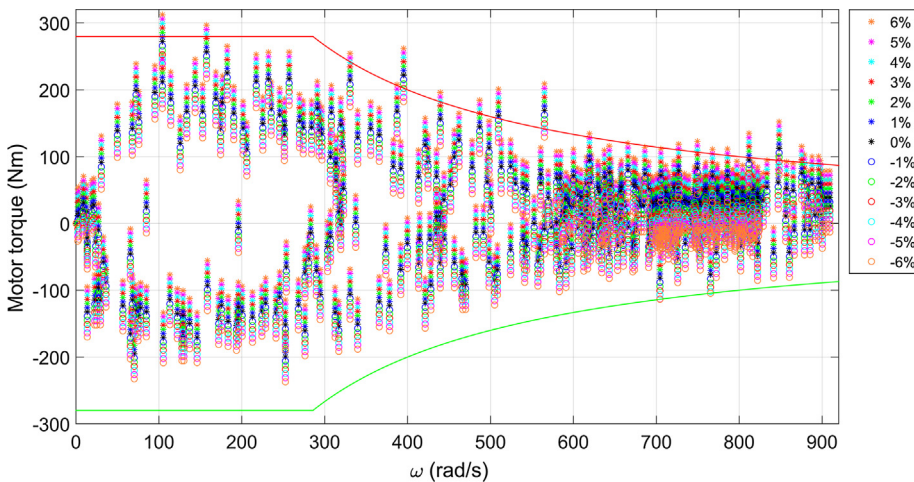


Fig. 21. Motor torque-speed plot for different road gradients over SFTP.

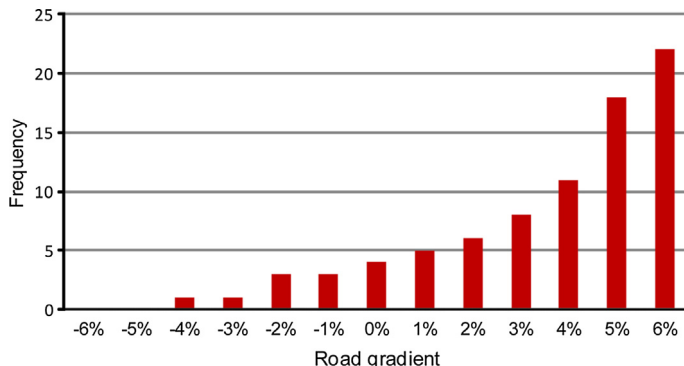


Fig. 22. Histogram of motor overload for different road gradients over SFTP.

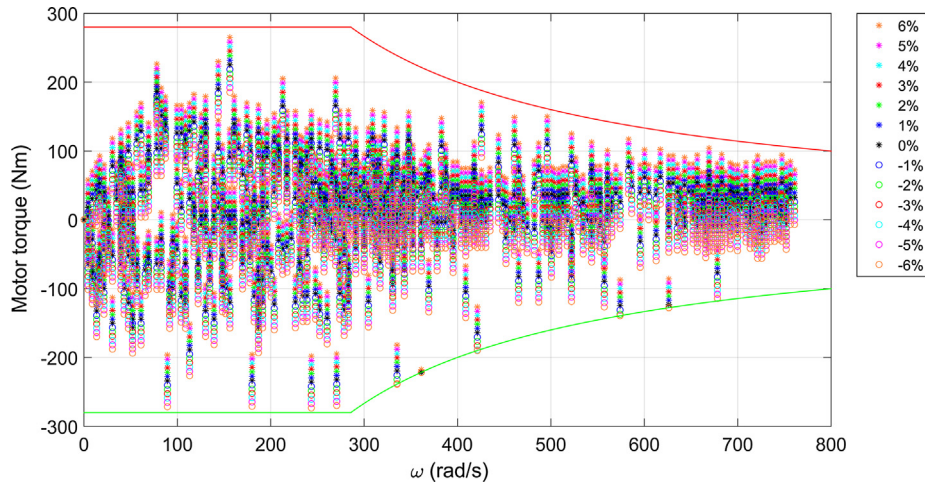


Fig. 23. Motor torque-speed plot for different road gradients over LA92-Short.

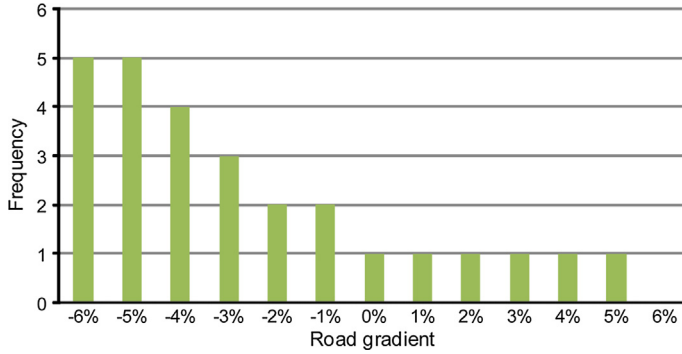


Fig. 24. Histogram of maximum energy regeneration for different road gradients over LA92-Short.

than the nominal one, mainly caused by the high deceleration at those instances. In this case, the redundant braking power is transformed into thermal energy by the mechanical brakes, while the generator achieves the maximum recoverable power and regenerates it, depending on its efficiency and vehicle speed.

The phenomenon where the available braking torque is larger than the torque that the electric motor can receive is more frequently observed during the simulation of the LA92-Short cycle, as shown in Fig. 23. In this light, the motor operates at its maximum regeneration capacity mostly for negative road gradients as expected, and more specifically it reaches the minimum torque limit 5 times for -5% and -6% road gradients (Fig. 24). It is also interesting to note that the mechanical braking system is activated even for positive road gradients up to the value of 5% . This fact can be exclusively explained by the high deceleration requirement in a particular instance of this aggressive driving cycle. Nevertheless, the operation points do not exceed the maximum torque curve while working as motor and the desired route is completed without overloading the electrical machine.

5. Conclusions

This paper presents the development of a computationally efficient simulation model for estimating the energy consumption of EVs. The proposed approach combines a generic physics-based vehicle model with high-level technical specifications of main EV components in order to transform the traction power requirements (at wheels) into EV battery power requirements. Key characteristics of the developed model include the dynamic approach to compute the energy recuperation as well as the capability of simulating motor overload conditions which can be observed under aggressive driving conditions and steep road slopes. For validation purposes, the output of the simulation model was compared with the results obtained from FASTSim over typical driving cycles with a test EV, confirming that it comprises a lightweight yet accurate implementation. Additional simulation results with different road gradients and highly demanding driving cycles provide useful insight on the capabilities of the proposed model and reveal that it can effectively capture the dynamics of EV operation.

In this framework, employing real-world driving profiles as input to the proposed model enables the fast computation of EV consumption factors with sufficient accuracy for EV route planning services running over large scale road networks, while the integration with routing applications running on mobile devices, which are typically characterized by low computational capabilities, provides a practical solution for assessing the EV trip consumption or estimating the energy-efficiency of suggested routes using real-time information of vehicle speed.

Acknowledgements

This work was supported by the European Commission through the FP7 Collaborative Project MOVESMART under grant agreement no. 609026.

References

- ANL (Argonne National Laboratory), 2016. AUTONOMIE <<http://www.autonomie.net/index.html>> (accessed 08.04.16).
- AVL, 2016. AVL Cruise – Vehicle System and Driveline Analysis <<http://www.avl.com/cruise>> (accessed 08.04.16).
- Barlow, T.J., Latham, S., McCrae, I.S., Boulter, P.G., 2009. A reference book of driving cycles for use in the measurement of road vehicle emissions. TRL Limited. Published Project Report PPR354.
- Baum, M., Dibbelt, J., Gemsa, A., Wagner, D., 2014. Towards route planning algorithms for electric vehicles with realistic constraints. *Comput. Sci. – Res. Dev.*, 1–5.
- Baum, M., Dibbelt, J., Pajor, T., Wagner, D., 2013. Energy-optimal routes for electric vehicles. In: Proceedings of the 21st ACM SIGSPATIAL International Conference on Advances in Geographic Information Systems. ACM, New York, NY, pp. 54–63.
- Brooker, A., Gonder, J., Wang, L., Wood, E., Lopp, S., Ramroth, L., 2015. FASTSim: A Model to Estimate Vehicle Efficiency, Cost and Performance. SAE 2015 World Congress & Exhibition, 21–23 April 2015, Detroit, Michigan.
- Campanari, S., Manzolini, G., Garcia de la Iglesia, F., 2009. Energy analysis of electric vehicles using batteries or fuel cells through well-to-wheel driving cycle simulations. *J. Power Sources* 186 (2), 464–477.
- Carsales.com.au, 2015. New 2014 Nissan LEAF ZE0 Auto Pricing and Specifications <<http://www.carsales.com.au/new-cars/details/Nissan-LEAF-2014/SHRM-AD-393592?sdmvc=1&intref=sr-bncis-model-stock>> (accessed 16.12.15).
- Ehsani, M., Gao, Y., Emadi, A., 2010. *Modern Electric Hybrid Electric and Fuel Cell Vehicles: Fundamentals, Theory, and Design*. Taylor & Francis, Boca Raton.
- European Commission, 2009. Commission Regulation (EC) No 640/2009 of 22 July 2009 implementing Directive 2005/32/EC of the European Parliament and of the Council with regard to ecodesign requirements for electric motors. Official Journal of the European Union, L 191/26.
- Fiori, C., Ahn, K., Rakha, H.A., 2016. Power-based electric vehicle energy consumption model: model development and validation. *Appl. Energy* 168, 257–268.
- Gao, Y., Ehsani, M., 2010. Design and control methodology of plug-in hybrid electric vehicles. *IEEE Trans. Industr. Electron.* 57 (2), 633–640.
- Howey, D.A., Martínez-Botas, R.F., Cussons, B., Lytton, L., 2011. Comparative measurements of the energy consumption of 51 electric, hybrid and internal combustion engine vehicles. *Transport. Res. Part D: Transp. Environ.* 16 (6), 459–464.
- IEA (International Energy Agency), 2013. Global EV Outlook 2013: Understanding the Electric Vehicle Landscape to 2020 <http://www.iea.org/publications/freepublications/publication/GlobalEVOutlook_2013.pdf> (accessed 16.12.15).
- IEA (International Energy Agency), 2015. Global EV Outlook 2015 <http://www.iea.org/evi/Global-EV-Outlook-2015-Update_1page.pdf> (accessed 16.12.15).
- INFRAS, 2015. HBFEA – Handbook Emission Factors for Road Transport <<http://www.hbefa.net/e/index.html>> (accessed 08.04.2016).
- Larminie, J., Lowry, J., 2012. *Electric Vehicle Technology Explained*. John Wiley & Sons Ltd, Chichester, United Kingdom.
- Li, Y., Zhang, L., Zheng, H., He, X., Peeta, S., Zheng, T., Li, Y., 2015. Evaluating the energy consumption of electric vehicles based on car-following model under non-lane discipline. *Nonlinear Dyn.* 82 (1–2), 629–641.
- Lorff, C., Martínez-Botas, R.F., Howey, D.A., Lytton, L., Cussons, B., 2013. Comparative analysis of the energy consumption and CO₂ emissions of 40 electric, plug-in hybrid electric, hybrid electric and internal combustion engine vehicles. *Transport. Res. Part D: Transp. Environ.* 23, 12–19.
- MOVESMART, 2016. MOVESMART: Renewable Mobility Services in Smart Cities <<http://www.movesmartfp7.eu/>> (accessed 08.04.2016).
- Muneeer, T., Milligan, R., Smith, I., Doyle, A., Pozuelo, M., Knez, M., 2015. Energetic, environmental and economic performance of electric vehicles: experimental evaluation. *Transport. Res. Part D: Transp. Environ.* 35, 40–61.
- Natural Resources Canada, 2004. Technical fact sheet-premium-efficiency motors Catalog No. M144-21/2003E. Office of Energy Efficiency, Energy Innovators Initiative, Ottawa.
- NREL (National Renewable Energy Laboratory), 2003. ADVISOR Advanced Vehicle Simulator <<http://adv-vehicle-sim.sourceforge.net/>> (accessed 08.04.16).
- NREL (National Renewable Energy Laboratory), 2014. FASTSim: Future Automotive Systems Technology Simulator <<http://www.nrel.gov/transportation/fastsim.html>> (accessed 08.04.16).
- Pellegrino, G., Vagati, A., Boazzo, B., Guglielmi, P., 2012a. Comparison of induction and PM synchronous motor drives for EV application including design examples. *IEEE Trans. Ind. Appl.* 48 (6), 2322–2332.
- Pellegrino, G., Vagati, A., Guglielmi, P., Boazzo, B., 2012b. Performance comparison between surface-mounted and interior PM motor drives for electric vehicle application. *IEEE Trans. Industr. Electron.* 59 (2), 803–811.
- Piller, S., Perrin, M., Jossen, A., 2001. Methods for state-of-charge determination and their applications. *J. Power Sources* 96 (1), 113–120.
- Qian, K., Zhou, C., Allan, M., Yuan, Y., 2011. Modeling of load demand due to EV battery charging in distribution systems. *IEEE Trans. Power Syst.* 26 (2), 802–810.
- Rahman, K.M., Ehsani, M., 1996. Performance analysis of electric motor drives for electric and hybrid electric vehicle applications. IEEE Workshop on Power Electronics in Transportation, Dearborn, 24–25 October 1996, pp. 49–56.
- Schellenberg, S., Berndt, R., Eckhoff, D., German, R., 2014. A computationally inexpensive battery model for the microscopic simulation of electric vehicles. IEEE Vehicular Technology Conference, Vancouver, BC, 14–17 September 2014, pp. 1–6.
- Schneider, M., Stenger, A., Goekke, D., 2014. The electric vehicle-routing problem with time windows and recharging stations. *Transport. Sci.* 48 (4), 500–520.
- Smith, W.J., 2010. Can EV (electric vehicles) address Ireland's CO₂ emissions from transport? *Energy* 35 (12), 4514–4521.
- Spichartz, P., Dost, P., Sourkounis, C., 2014. Recuperation strategies for electric vehicles. 9th International Conference on Ecological Vehicles and Renewable Energies (EVER 2014), Monte-Carlo, 25–27 March 2014, pp. 1–7.
- Travasset-Baro, O., Rosas-Casals, M., Jover, E., 2015. Transport energy consumption in mountainous roads. A comparative case study for internal combustion engines and electric vehicles in Andorra. *Transport. Res. Part D: Transp. Environ.* 34, 16–26.
- U.S. Department of Energy, 1997. Determining Electric Motor Load and Efficiency <<http://www.energy.gov/sites/prod/files/2014/04/f15/10097517.pdf>> (accessed 16.12.15).
- U.S. Department of Energy, 2014. Premium Efficiency Motor Selection and Application Guide – A Handbook for Industry. Office of Energy Efficiency and Renewable Energy. Available at: http://www.energy.gov/sites/prod/files/2014/04/f15/amo_motors_handbook_web.pdf.
- U.S. Environmental Protection Agency, 2013. Dynamometer Drive Schedules <<http://www.epa.gov/nvfel/testing/dynamometer.htm>> (accessed 16.12.15).

- Vagati, A., Pellegrino, G., Guglielmi, P., 2010. Comparison between SPM and IPM motor drives for EV application. XIX International Conference on Electrical Machines (ICEM 2010), Rome, 6–8 September 2010, pp. 1–6.
- Van Sterkenburg, S., Rietveld, E., Rieck, F., Veenhuizen, B., Bosma, H., 2011. Analysis of regenerative braking efficiency – a case study of two electric vehicles operating in the Rotterdam area. 2011 IEEE Vehicle Power and Propulsion Conference (VPPC 2011), Chicago, IL, 6–9 September 2011, pp. 1–6.
- Vodovozov, V., Raud, Z., Lehtila, T., Rassolkin, A., Lillo, N., 2014. Comparative analysis of electric drives met for vehicle propulsion. In: 9th International Conference on Ecological Vehicles and Renewable Energies (EVER 2014), Monte-Carlo, 25–27 March 2014, pp. 1–8.
- Wu, X., Freese, D., Cabrera, A., Kitch, W.A., 2015. Electric vehicles' energy consumption measurement and estimation. *Transport. Res. Part D: Transp. Environ.* 34, 52–67.
- Yang, H., Yang, S., Xu, Y., Cao, E., Lai, M., Dong, Z., 2015. Electric vehicle route optimization considering time-of-use electricity price by learnable Parthenogenetic algorithm. *IEEE Trans. Smart Grid* 6 (2), 657–666.
- Yang, S., Deng, C., Tang, T., Qian, Y., 2013. Electric vehicle's energy consumption of car-following models. *Nonlinear Dyn.* 71 (1–2), 323–329.
- Yao, E., Wang, M., Song, Y., Yang, Y., 2013. State of charge estimation based on microscopic driving parameters for electric vehicle's battery. *Math. Prob. Eng.*
- Yeo, H., Kim, D., Hwang, S., Kim, H., 2004. Regenerative braking algorithm for a HEV with CVT ratio control during deceleration. In: International Continuously Variable and Hybrid Transmission Congress, San Francisco, 23–25 September 2004.
- Yildirim, M., Polat, M., Kurum, H., 2014. A survey on comparison of electric motor types and drives used for electric vehicles. In: 16th International Power Electronics and Motion Control Conference and Exposition (PEMC 2014), Antalya, 21–24 September 2014, pp. 218–223.
- Zhang, R., Yao, E., 2015. Electric vehicles' energy consumption estimation with real driving condition data. *Transport. Res. Part D: Transp. Environ.* 41, 177–187.